Published in final edited form as:
Nature. 2013 November 07; 503(7474): 115–120. doi:10.1038/nature12600.

Dendritic spikes enhance stimulus selectivity in cortical neurons *in vivo*

Spencer L. Smith[1,2], **Ikuko T. Smith**[1,2], **Tiago Branco**[1,3], and **Michael Häusser**[1]

[1]Wolfson Institute for Biomedical Research and Department of Neuroscience, Physiology and Pharmacology, University College London, Gower Street, London WC1E 6BT, UK

[2]Department of Cell Biology and Physiology and Neuroscience Center, University of North Carolina School of Medicine, Chapel Hill, North Carolina 27599, USA

[3]Laboratory of Molecular Biology, Medical Research Council, Cambridge CB2 0QH, UK

Abstract

Neuronal dendrites are electrically excitable: they can generate regenerative events such as dendritic spikes in response to sufficiently strong synaptic input1–3. Although such events have been observed in many neuronal types4–9, how active dendrites contribute to tuning of neuronal output *in vivo* is not well understood. Here we have addressed this question by performing direct patch-clamp recordings from the dendrites of pyramidal neurons in primary visual cortex during sensory processing in lightly anesthetized and awake mice. Visual stimulation triggered regenerative events that included dendritic spikes. These events were orientation tuned and suppressed by either hyperpolarization or intracellular NMDA receptor blockade. Both of these manipulations also decreased the selectivity of subthreshold orientation tuning measured at the soma, thus linking dendritic regenerative events with somatic orientation tuning. Together, our results suggest that dendritic spikes triggered by visual input contribute to a fundamental cortical computation: enhancing orientation selectivity in visual cortex.

Neuronal dendrites express voltage-dependent Ca^{2+} and Na^{+} channels that confer electrical excitability, in particular the ability to support active backpropagation of action potentials and the initiation of local dendritic spikes1. In addition, the voltage-dependent Mg^{2+} block of synaptic NMDA receptors can also support nonlinear synaptic integration and dendritic spike initiation5,10. These mechanisms of active synaptic integration have been probed extensively *in vitro*2. Although dendritic spikes have been observed *in vivo* under some conditions6–8, it remains unclear whether these mechanisms are involved in behaviorally relevant computations11–13. To investigate whether dendritic nonlinearities can contribute to a well-known example of cortical computation, orientation tuning in the visual cortex14,

Corresponding authors: Spencer L. Smith (slab@unc.edu) and Michael Häusser (m.hausser@ucl.ac.uk); Address for editorial correspondence: Michael Häusser, Wolfson Institute for Biomedical Research, University College London, Gower Street, London WC1E 6BT, UK, tel. +44-(0)20-7679-6756, fax +44-(0)20-7679-6878, m.hausser@ucl.ac.uk.

Author Contributions

S.L.S. and M.H. conceived and designed the experiments. S.L.S. and I.T.S. performed the experiments. S.L.S. analyzed the data. T.B. designed and carried out the compartmental modeling. S.L.S., I.T.S., T.B., and M.H. interpreted the data and wrote the paper.

Europe PMC Funders Author Manuscripts

we have made direct dendritic patch clamp recordings from layer 2/3 neurons in mouse visual cortex.

To measure dendritic activity *in vivo*, whole-cell patch-clamp recordings were obtained from the thin (diameter: 2.0 ± 0.4 μm, mean ± S.D., $n = 12$) apical dendrites of layer 2/3 neurons in mouse primary visual cortex (Fig. 1a) in lightly anesthetized and awake mice. Cells were filled via the patch pipette with a fluorescent Ca^{2+} dye (Oregon Green BAPTA-1, 100 μM) for imaging Ca^{2+} transients, and a fluorescent red dye (Alexa 594, 25-50 μM) to image the morphology of the dendritic arbor and identify the precise location of the dendritic recording (Fig. 1b). Dendritic recordings exhibited expected physiological features, such as a high local input resistance increasing with distance from the soma (Extended Data Fig. 1a-c)15,16.

In somatic recordings, visual stimulation with drifting square wave gratings evoked conventional action potential activity, with the firing rate tuned to the orientation of the stimulus (Fig. 1c)14,17. By contrast, recordings from distal dendrites (>75 μm from the soma) revealed orientation-tuned, high frequency bursts of Na^+ spikes riding on a depolarization envelope consistent with activation of voltage-gated Ca^{2+} channels and synaptic NMDAR currents (Fig. 1d-g, Extended Data Fig. 1d). Their properties contrasted with those of isolated spikes (single spikes separated by at least 50 ms from other spikes), which are presumed to be backpropagating action potentials (bAPs; Fig. 1d, e), though not all bAPs are isolated bAPs. These isolated bAPs exhibited a uniform amplitude and shape within a recording, and decreased in amplitude and increased in width with increasing distance from the soma (Extended Data Fig. 1e-f)15. While dendritic bursts can contain both local Na^+ spikes and bAPs, these isolated bAPs provide a readout of somatic activity that can be compared with local dendritic events. Visually evoked spike bursts recorded at the dendrite were tuned to the orientation of the stimulus, with reliable tuning trial-to-trial (Fig. 1e, f). The preferred orientation of bursts was not different from that of bAPs ($n = 9$, difference in preferred orientation: 34.7 ± 28.8°; $P = 0.22$, paired t-test; Extended Data Fig. 2).

We next sought to determine whether these dendritic events were local. Given that Na^+ spikes, a prominent feature of the dendritic regenerative events we recorded, have fast kinetics, their waveform is likely to be heavily attenuated by the cable filtering properties of the dendritic arbor, and thus not propagated efficiently to the soma (by contrast, the slow depolarization envelope of dendritic regenerative events can propagate to the soma). The maximum instantaneous and mean spike rates, as well as the variance-to-mean ratio, were highest in distal dendritic (> 75 μm; $n = 9$) recordings compared to proximal dendritic (< 50 μm; $n = 5$) or somatic recordings, suggesting that many of the individual spikes in bursts observed in distal dendritic recordings are indeed local dendritic spikes and not bAPs15. Spike statistics from somatic recordings and proximal (< 50 μm from the soma; mean diameter ± S.D.: 1.7 ± 0.3 μm, $P = 0.14$, two sample t-test, not different from the diameter of distal dendrites recorded) dendritic recordings were indistinguishable ($P > 0.05$; two sample t-test), thus confirming that the dendritic recording configuration itself does not affect spike rates. These measurements were made in lightly anesthetized mice, and similar spiking patterns were observed in dendritic recordings from awake mice (Fig. 2a, filled symbols;

Extended Data Fig. 3), demonstrating that such spiking is also present in the alert, behaving animal. These data indicate that, at distal dendritic recording sites, spiking occurs at higher rates and with a higher degree of “burstiness” than spiking recorded at the soma, and provide the first piece of evidence that these dendritic events are local.

A second piece of evidence indicating the dendritic origin of these events is provided by the onset, or foot of the spike waveform. A signature of propagated spikes is a sharp inflection at the foot of the spike, in contrast to the smooth rise observed near the site of spike initiation18. Isolated spontaneous spikes exhibited a clear ‘kink’, as expected for backpropagated APs (Fig. 2b). Spikes within bursts, in contrast, generally exhibited a much slower onset, indicative of local generation (Fig. 2c). The membrane potential at spike initiation did not completely predict the spike onset speed (Extended Data Fig. 4). Thus, the depolarization envelope during dendritic bursts, which can also slow spike onset, did not alone account for the difference in spike shape. Although these spikes were heterogeneous and likely a mixed population containing some bAPs, across the population, spikes within bursts consistently exhibited a slower onset ($P = 0.0013$, Wilcoxon rank sum test, $n = 7$; data from awake mice exhibited the same trend, Fig. 2d), consistent with their identity as locally generated dendritic spikes.

To obtain a third piece of evidence, and a more direct readout of the relationship between dendritic spikes and somatic action potentials, we used two photon calcium imaging to simultaneously measure calcium fluctuations at the soma, allowing us to infer somatic action potential activity during dendritic patch recordings. Spike bursts recorded at distal dendritic sites were correlated with somatic calcium signals (Fig. 3a). As was the case with the tuning of dendritic bursts and bAPs, the preferred orientation of dendritic bursts (Fig. 3b) was similar to the preferred orientation of the somatic calcium signal (Fig. 3c), with qualitative differences in the tuning curves consistent with the interpretation that a single dendrite contributes only a portion of the input that drives a neuron to fire. To calibrate these measurements, we used separate somatic recordings combined with somatic calcium imaging. The somatic calcium signal observed during a dendritic burst of 4-5 spikes was indistinguishable from the calcium signal observed during a single action potential recorded at the soma ($P = 0.77$, two sample t-test; Fig. 3d). Furthermore, although the somatic calcium signals saturated near the same level (30% $\Delta F/F$, $P = 0.99$, two-sample t-test) in both dendritic and somatic recording configurations, this saturation level was reached with just 10 spikes recorded at the soma, and took more than 40 spikes in the dendrite (two distributions are different, $P < 10^{-8}$, $n = 5$, multivariate Kolmorogov-Smirnov test; Fig. 3e). Thus, many of the individual spikes in bursts recorded at the dendrite were likely locally generated rather than each reflecting a bAP, and resulted in subthreshold depolarizations at the soma. Measurements of calcium signals at the site of distal dendritic recordings (Extended Data Fig. 5a) provided further evidence, showing that dendritic bursts with calcium signals spanning all visible dendritic branches (Extended Data Fig. 5b) contained spikes with steeper onsets than bursts with calcium transients confined to the local recording site, and not observed in adjacent branches (Extended Data Fig. 5c-f, $n = 78$ dendritic bursts)19. Together, these results demonstrate how dendritic spikes, local calcium, and bAPs interact during visual processing.

A final piece of evidence that dendritic bursts consist of locally generated dendritic spikes is that visually evoked dendritic bursts were more sensitive to local dendritic hyperpolarization than bAPs. When steady hyperpolarizing current was delivered via the dendritic patch pipette, the rate of burst events decreased more than the rate of isolated bAPs ($P = 0.005$, paired t-test; Fig. 4), indicating that dendritic burst-generating mechanisms were more sensitive to local membrane potential than those mechanisms that support backpropagation of somatic action potentials. Taken together, these findings indicate that the spike bursts recorded at the dendrite during visual processing are not a pure population of bAPs, but rather consist primarily of locally generated dendritic spikes.

How might dendritic regenerative events evoked by visual stimulation influence orientation tuning of neuronal output? The prolonged depolarization envelope of dendritic bursts can propagate to the soma and influence axonal output. If these events are required for normal synaptic integration during visual processing, then blocking them may disrupt an important cortical computation: orientation tuning. Layer 2/3 neurons exhibited robustly orientation tuned spiking17 and subthreshold responses (Fig. 5a-d; even when cells fire few to no spikes, Extended Data Fig. 6). Subthreshold tuning closely matched the spike-based tuning in terms of preferred orientation (Pearson's $R = 0.83$, $P < 10^{-5}$; Extended Data Fig. 7a)20 and orientation selectivity (membrane potential orientation selectivity index, V_mOSI; Pearson's $R = 0.88$, $P = 0.0040$; Extended Data Fig. 7b). This subthreshold tuning provides a way to examine synaptic integration in both the control and hyperpolarized conditions, where dendritic spikes are prevented (Fig. 4). Hyperpolarization degraded this subthreshold orientation tuning both in the modulation amplitude (Fig. 5e,f), and selectivity (Fig. 5g) without changing the preferred orientation ($n = 10$, Pearson's $R = 0.88$, $P = 0.022$; Extended Data Fig. 7c-d). This effect was not accounted for by changes in the driving force for Cl^- ($R = 0.34$; $P = 0.15$; Extended Data Fig. 8). These results demonstrate that voltage-gated mechanisms are required for normal synaptic integration and subthreshold orientation tuning during visual processing, which is consistent with the hypothesis that dendritic regenerative events enhance subthreshold orientation tuning.

Synaptic NMDA receptor current, which is subject to a voltage-dependent Mg^{2+} block, is a prime candidate for linking synaptic input to regenerative events on dendrites10,15. Visually-driven synaptic input to layer 2/3 pyramidal cells activates synaptic NMDA receptors21. To determine whether NMDA receptors may be one of the voltage-dependent mechanisms that contributes to nonlinear synaptic integration *in vivo*, we used whole cell somatic recordings with a use-dependent, intracellular NMDA receptor blocker, MK-801, included in the pipette solution22. Intracellular MK-801 did not affect Up and Down state dynamics (Extended Data Fig. 9a-b), confirming that the manipulation was restricted to the recorded cell, and dendritic spiking in the recorded cell was blocked by MK-801 (Extended Data Fig. 9c-d). Early in these recordings, prior to effective NMDA receptor block, subthreshold orientation tuning was normal, but late in the recordings, after MK 801 had diffused through the dendritic tree, V_mOSI decreased markedly (Fig. 5h-j), as did spike-based tuning (OSI early in recording: 0.82 ± 0.12, late in recording: 0.45 ± 0.17; $P = 0.016$; paired t-test; $n = 5$; Fig. 5i-j). Since the orientation selectivity was degraded, despite the remaining, unblocked receptor pathways (e.g., AMPA and metabotropic glutamate receptors), we conclude that NMDA receptor currents are crucial for the tuning of synaptic

integration in these neurons and their depolarization-dependent relief from Mg^{2+}-block may be a key mechanism linking synaptic input and dendritic regenerative events including dendritic spikes5,10.

We have presented multiple lines of evidence, including direct dendritic recordings, to reveal that visually evoked sensory input triggers local dendritic spikes in cortical pyramidal neurons *in vivo*. Moreover, hyperpolarization decreased both the rate of dendritic spiking and V_mOSI, thus demonstrating that voltage-dependent dendritic mechanisms help shape the input-output function of neurons during sensory processing23. Finally, we have also provided evidence for at least one specific biophysical mechanism, NMDA receptors, which can underlie these dendritic events. Together, these results show that synaptic integration of sensory input crucially relies on voltage-dependent dendritic mechanisms.

A detailed compartmental model of layer 2/3 pyramidal cells confirmed that a biophysically plausible model can account for our data (Supplementary Note 1, Extended Data Fig. 10, Supplementary Videos 1-3). This model reproduced the key findings of this study and offers potential mechanistic insights. For example, passively propagated Na^+ spikes can arrive just after an actively generated spike on a dendrite and support instantaneous spike rates of several hundred Hz, as observed in distal dendritic recordings (Fig. 2a). Also, cooperative recruitment of NMDA receptor current provides a crucial link between synaptic input and fast dendritic spiking. These results show that basic biophysical mechanisms support the electrophysiological phenomena we observed in direct dendritic recordings in vivo.

Our experimental results and compartmental modeling suggests that synaptic input causes a dendritic depolarization that activates voltage-dependent ion channels and relieves the Mg^{2+} block of NMDA receptors5,10,15. This results in a supralinear, local regenerative event that includes dendritic Na^+ spikes. The slow time course of the NMDA receptor current component of the regenerative events causes a prolonged depolarization envelope that propagates to the soma, and enhances axonal output. Thus, local computational subunits generated by voltage-dependent mechanisms in dendrites22,24 are activated by sensory input *in vivo*, provide an orientation-tuned signal to the soma, and thereby help determine stimulus selectivity.

Dendritic regenerative events provide a mechanism by which a relatively small number of inputs can drive spike output24,25, changing effective connectivity between local functional groups of neurons26, or mitigating the noise in cortical circuits27, by ensuring that variable synaptic input can result in a more reliable postsynaptic response. Our data from awake experiments demonstrates that these dendritic events occur during alert sensory processing28. Since dendrite-targeting inhibitory interneurons are inhibited in awake mice during sensory stimulation29, this circuitry may play a key role in gating sensory input30. Overall, our results demonstrate that dendrites are not passive integrators of sensory-driven input *in vivo*. Rather, sensory input engages dendritic voltage-dependent mechanisms to generate local regenerative events and dendritic spikes, which play an important role in shaping orientation selectivity, a quintessential cortical computation.

Europe PMC Funders Author Manuscripts

Methods Summary

Wild-type C57/blk6 mice (24-56 days old, both male and female) were anesthetized with isoflurane (5% for induction, 1.5 - 2.5% for surgery, 0 - 0.5% during recording), augmented with chlorprothixene (0.5 - 2 mg/kg). Experiments with awake mice were carried out during head fixation, during which mice would freely move their limbs, groom, and drink a sweet liquid reward when offered. Square-wave gratings (0.04 cycles/°, 2 cycles/s) were displayed on an LCD screen to map orientation selectivity. The screen was shrouded with a cone up to the eye of the mouse to prevent contamination of the imaging pathway with light from the visual stimulus. For both dendritic and somatic recordings, the pipette solution contained (in mM): 140 or 135 $KMeSO_4$, 4 or 10 KCl, 10 HEPES, 10 Na_2-phosphocreatine, 4 Mg-ATP, 0.3 Na_3-GTP, 0.1 Oregon Green BAPTA-1, 0.025 - 0.050 Alexa 594; pH adjusted with KOH to 7.2; 290 mOsm. Pipette resistances ranged from 4.9 to 11 MΩ (mean = 7.9 MΩ) for dendritic recordings, and from 5 to 8 MΩ (mean = 6.9 MΩ) for somatic recordings. All recordings were from the apical dendrites of superficial layer 2/3 pyramidal neurons. Unlike layer 5 or deeper layer 2/3 neurons, these neurons do not have a prominent apical trunk and tuft do, so recorded dendrites were geometrically similar to basal dendrites. A custom-built two-photon microscope with a 16x magnification and 0.8 numerical aperture water immersion objective (Nikon) and a large aperture collection pathway was used to image neurons. In dendritic recordings, putative bAPs were automatically identified as single spikes when isolated from other spikes by at least 50 ms. Unless otherwise specified, all measurements are expressed as mean ± S.E.M.

Online Methods

Preparation

All experiments were carried out in accordance with the regulations of the UK Home Office, or the guidelines and regulations of the US Department of Health and Human Services, and the University of North Carolina. Wild-type C57/blk6 mice (24-56 days old) were anesthetized with isoflurane (5% for induction, 1.5 – 2.5% for surgery, 0 – 0.5% during recording), augmented with chlorprothixene (0.5 – 2 mg/kg). During recording, this regime resulted in a sedated state where the animal was not voluntarily moving, but would still respond to a toe pinch. Increased levels of isoflurane (> 0.5%) typically suppressed spiking activity, including dendritic bursts. Experiments with awake mice were carried out during head fixation, during which mice would routinely move their limbs, groom, and drink a sweet liquid reward when offered.

After gluing a headplate to the skull for head fixation during surgery and recording, a 2-3 mm diameter craniotomy was opened over monocular visual cortex. A thin layer of agar (1.5%) dissolved in artifical cerebrospinal fluid (in mM: 150 NaCl, 2.5 KCl, 10 HEPES, 2 $CaCl_2$, 1 $MgCl_2$; pH adjusted with NaOH to 7.3; 300 mOsm) and placed on top of the brain helped dampen movement. A homeothermic heat pad maintained body temperature within the physiological range. Water-based opthalmic ointment maintained eye health.

Visual stimulation

Visual stimulus presentation was controlled by routines written in MATLAB using the Psychophysics Toolbox extensions31,32. Square-wave gratings (0.04 cycles/°, 2 cycles/s) of black (2 cd/m^2) and white (86 cd/m^2) bars in eight different orientations were displayed on an LCD screen (ESAW 7 inch VGA TFT, set at 1024 × 768 resolution and 60 Hz refresh rate) to map orientation selectivity. The screen was shrouded with a cone up to the eye of the mouse to prevent contamination of the imaging pathway with light from the visual stimulus. The visual stimulus extended from +20° to +124° in azimuth and from -10° to +42° in elevation. Visual stimuli were presented in a shuffled order: each orientation was presented one time per sweep of 8 orientations, and the order of the orientations was different for each sweep.

Patch-clamp recordings

For both dendritic and somatic recordings, the pipette solution contained (in mM): 140 or 135 $KMeSO_4$, 4 or 10 KCl, 10 HEPES, 10 Na_2-phosphocreatine, 4 Mg-ATP, 0.3 Na_3-GTP, 0.1 Oregon Green BAPTA-1, 0.025-0.050 Alexa 594; pH adjusted with KOH to 7.2; 290 mOsm. Pipette resistances ranged from 4.9 to 11 MΩ (mean = 7.9 MΩ) for dendritic recordings, and from 5 to 8 MΩ (mean = 6.9 MΩ) for somatic recordings. For dendritic recordings, imaging33 was used to guide the pipette away from blood vessels and somata, and tip resistance measured using a voltage step in voltage-clamp mode was used to detect contact with a dendrite. Shadowpatching techniques33 were used to directly target the pipette to the soma. In somatic hyperpolarization experiments, cells were hyperpolarized by 21.4 ± 11.4 mV (mean ± SD; from a membrane potential of -49.4 ± 6.7 mV to -70.8 ± 9.4 mV, mean ± SD; average V_m across all stimuli after removing spikes). All dendritic recordings were from the apical dendrites of superficial layer 2/3 pyramidal neurons. These neurons do not have a large apical trunk and tuft, as layer 5 or deeper layer 2/3 neurons do, so recorded dendrites were geometrically similar to basal dendrites. Series resistance was 39 ± 5 MΩ and 34 ± 5 MΩ for dendritic and somatic recordings, respectively. Series resistance did not change as a function of dendritic distance from the soma (r = -0.24, P = 0.50, n = 13). The bridge was rebalanced as needed during the recording. R_{series} increased less than 2% over the time it took to run a tuning curve. In one case, we obtained two distal dendritic recordings in the same mouse. In all other cases, we obtained at most one distal dendritic recording per mouse.

Compartmental modeling

Simulations were performed with the NEURON simulation environment (version 7.2) using a detailed reconstruction of a biocytin-filled L2 pyramidal neuron (Martin, K; NeuroMorpho.org ID NMO_00904). Passive parameters were C_m = 1 μF/cm^2, R_m = 7,000 Ω·cm^2, R_i = 100 Ω·cm, yielding a somatic input resistance of 110 MΩ, similar to the experimentally measured mean value (Supplementary Fig. 1a). AMPA, NMDA and $GABA_A$ synapses had a peak conductance of 1 nS and were modeled as a bi-exponential function, with time constants of (in ms). AMPAtau1 = 0.1, AMPAtau2 = 1, NMDAtau1 = 2, NMDAtau2 = 20, $GABA_A$tau1 = 0.1, $GABA_A$tau2 = 4 (inhibition reversal potential was set to -80 mV). The magnesium block of NMDA synapses was modeled according to Jahr and

Stevens34. Active conductances were introduced in the soma and in all dendritic compartments, and included (mS/cm^2): voltage-activated sodium channels (soma 100, dendrite 60, distributed as a hot-spot in the center of each branch)35; high-voltage activated calcium channels (soma 0.05, dendrite 0.05); low-voltage activated calcium channels (soma $0.3x10^{-3}$, dendrite $0.15x10^{-3}$); voltage-activated potassium channels (10 soma; 0.3 dendrite); M-type potassium channels (soma 0.22, dendrite 0.1); calcium-activated potassium channels (soma 0.3, dendrite 0.3). Dendritic calcium was modeled by adding the current carried by voltage-activated calcium channels and the calcium fraction of the NMDA current (10%)36 and convolving it with a decaying exponential with a 50 ms time constant.

A total of 1100 synapses were randomly distributed across the dendritic tree, 80% excitatory and 20% inhibitory. Synapses were separated into background and signal synapses (signal was 10% of the total synapse number) and were activated with independent Poisson trains delivered to each synapse. Background synapses were continuously activated at a mean rate of 0.5 Hz, and signal synaptic input was activated at 5-8 Hz after a 200 ms baseline, and stayed active for 200 ms. The results did not depend on the total number of synapses, but rather the total input rate. For example, 100 synapses activated at 1 Hz yielded the same result as 1000 synapses activated at 0.1 Hz (the model did not include short-term plasticity).

Imaging

A custom-built two-photon microscope using galvanometer-based scan mirrors (6 mm diameter, Cambridge Technologies) with a 16 x magnification and 0.8 numerical aperture water immersion objective (Nikon) and a large aperture collection pathway with low-noise photomultiplier tubes (models 3896 and 7422-40P, Hamamatsu) was used to image neurons. Frame scans (15.6 frames/s) and line scans (1 ms/line) were acquired using ScanImage37.

Analysis

General—Custom programs written for MATLAB (MathWorks) and Igor Pro (Wavemetrics), including event detection and analysis routines in Igor by Taro Ishikawa (Jikei University), were used for analysis. Input resistance was measured as the steady state membrane potential in response to a current step. Maximum instantaneous firing rates were computed as the reciprocal of the smallest interspike interval. In dendritic recordings, putative bAPs were automatically identified as single spikes when isolated from other spikes by at least 50 ms.

Statistics—Unless otherwise specified, all measurements are expressed as mean ± S.E.M. The Shapiro-Wilk test was used to confirm, prior to application of two-sided parametric tests, that the deviation from normality of the data was statistically insignificant. For non-normal data, or data with significantly different variances, non-parametric tests were used as noted in the text (e.g., the Wilcoxon rank sum test is used in Fig. 2). The multivariate Kolmorogov-Smirnov test was computed using the generalization of Fasano and Franceschini38. Experimental manipulations (hyperpolarization and MK-801 block of NMDA receptors), did not involve randomization or blinding because each recorded cell served as its own control (control vs. hyperpolarized, or early vs. late recording, respectively). Sample sizes were designed to reliably measure neurophysiological

parameters while remaining in compliance with ethical guidelines to minimize the number of animals used. Results from Fig. 2a remain statistically significant ($P < 0.05$) when the top 1-2 data points from distal dendritic recordings are omitted from analysis. To test the statistical significance of orientation tuning of dendritic bursts, we first computed the OSI of the measured dendritic burst firing. We then shuffled the responses so that their associated orientation was assigned at random. We then computed the OSI of the new, reshuffled responses. This procedure was repeated 1000 times. The P value was taken as the fraction of time a randomly shuffled response yielded an OSI equal to or greater than the actual response.

Orientation tuning analysis—Orientation selectivity index was computed after fitting a sum of two Gaussian curves to the orientation tuning curve (whether based on spiking or membrane potential), with the centers 180° apart:

$$OSI = \frac{(Rp - Ro)}{(Rp + Ro)}$$

Where Rp is the response to the preferred orientation and Ro is the response at the orthogonal orientation. Cells in which the sum of squared residuals between the Gaussian fit and the observed data was less than 15% of the maximum value of the Gaussian fit were considered to be well described by the Gaussian fit.

Membrane potential (V_m) modulation in response to visual stimuli was computed by taking the peak-to-trough amplitude of the cycle average at 2 Hz (the drift rate of the visual stimulus gratings) of the membrane potential response (after removing any spikes). This modulation can be seen in the traces of Fig. 5c, particularly at 135° and 315°.

Europe PMC Funders Author Manuscripts

Extended Data

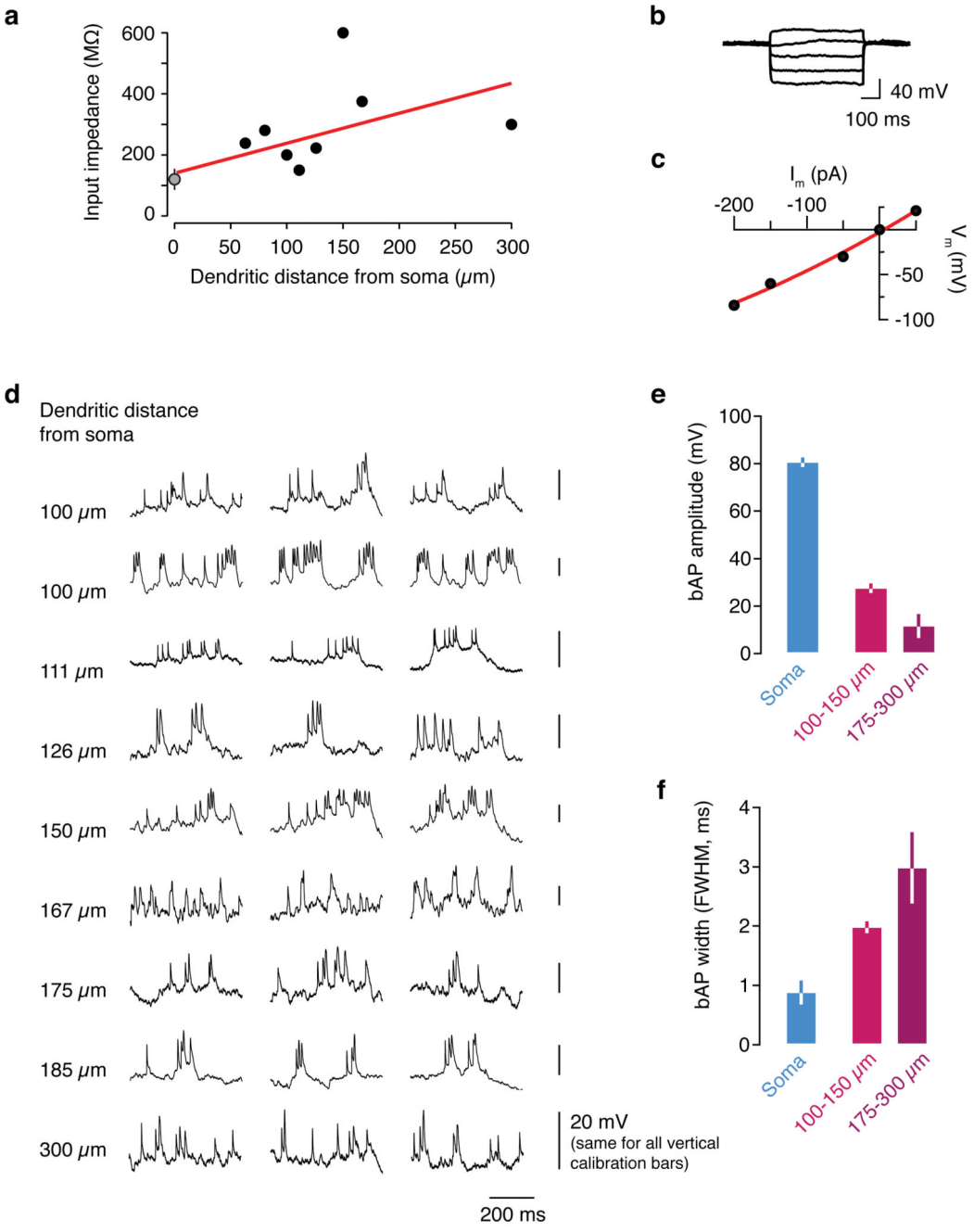

Extended Data Figure 1. Electrophysiological features of L2/3 dendrites *in vivo*.

a, The input resistance of distal dendrites was typically 100-300 MΩ, sometimes larger (up to 600 MΩ). Input resistance increased as function of dendritic distance from the soma, approximately doubling every 300 μm. The grey point indicates the input resistance measured in somatic patch clamp recordings (mean ± S.E.M). **b**, During a dendritic recording 150 μm from the soma, hyperpolarizing current steps did not reveal a voltage sag,

thus there is likely little to no hyperpolarization-activated cation current, I_h, in the dendrites of layer 2/3 pyramidal neurons *in vivo*. **c**, The peak voltage response plotted against hyperpolarizing current step amplitude in an I-V plot was well fit by a linear function, confirming the lack of I_h. **d**, Representative dendritic bursts evoked by visual stimulation at the optimal orientation in 9 different dendritic recordings at progressively further distances from the soma. All right-hand scale bars are 20 mV. **e**, Compared to action potentials recorded at the soma, bAPs were lower amplitude, and **f**, prolonged in time, and both of these trends were more pronounced with increasing dendritic distance from the soma (error bars indicate S.D.). Both the amplitude and width were significantly different among the three groups ($P < 0.01$, unpaired t-tests with the Bonferroni correction for multiple comparisons).

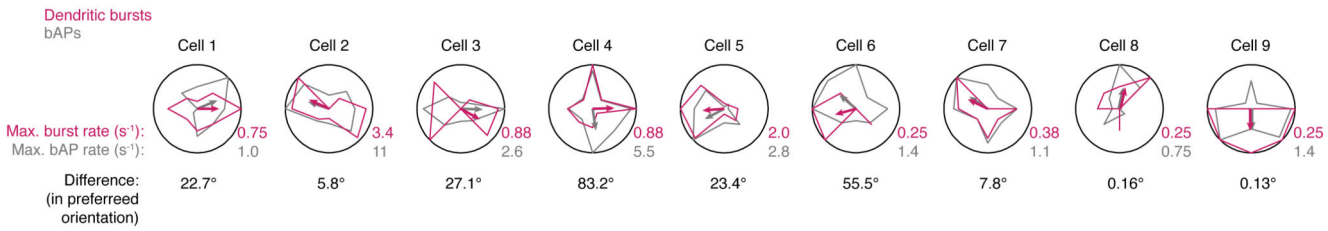

Extended Data Figure 2. Orientation tuning curves of dendritic bursts compared to bAPs.
Tuning curves for dendritic spike bursts and bAPs recorded at distal dendritic locations (> 75 μm from soma). Tuning curves for dendritic bursts match the tuning curves for isolated bAPs. The statistical significance of dendritic burst tuning curves were tested by randomly shuffling responses (details in Supplementary Methods) and found to be significant ($P < 0.05$) for 7 out of 9 cells (dendritic burst tuning in cells 6 and 9 were not significant). Curves are normalized to maximal values, shown at the bottom right of each polar plot. The small qualitative differences may be due to dendrites topologically distant from the dendritic recording site exhibiting slightly different tuning curves. The grating drift direction that elicited the largest response is indicated with an arrow. The difference between these directions between is indicated at the bottom of each polar plot. The cross correlation between dendritic bursts and isolated bAPs was highly significant: $R = 0.54$, $P = 0.000013$, $n = 9$, paired t-test. When only the spikes in bursts with rise times in the slowest quartile of the distribution were considered dendritic in origin, the preferred orientation of bAPs and the slowest quartile were still matched within individual dendritic recordings (difference in preferred orientation: 41.5 ± 58.1°, $P = 0.49$, $n = 9$, paired t-test).

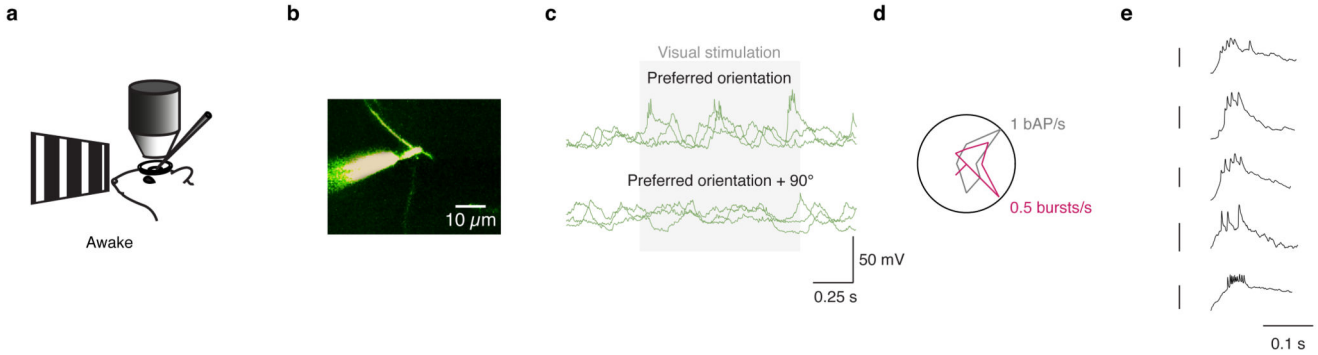

Extended Data Figure 3. Dendritic recordings in awake mice exhibit dendritic bursts.

a, Awake, headfixed mice viewed drifting gratings during electrophysiological recordings. **b**, Two photon image of the patched dendrite of a layer 2/3 pyramidal neuron in mouse visual cortex filled with Alexa 594 via the dendritic patch clamp pipette (117 μm from the soma). **c**, Dendritic bursts were observed when the preferred orientation was presented. **d**, Tuning curves for the isolated bAPs and dendritic bursts. **e**, Example bursts from three different distal dendritic recordings in awake mice. Calibration bars are 25 mV.

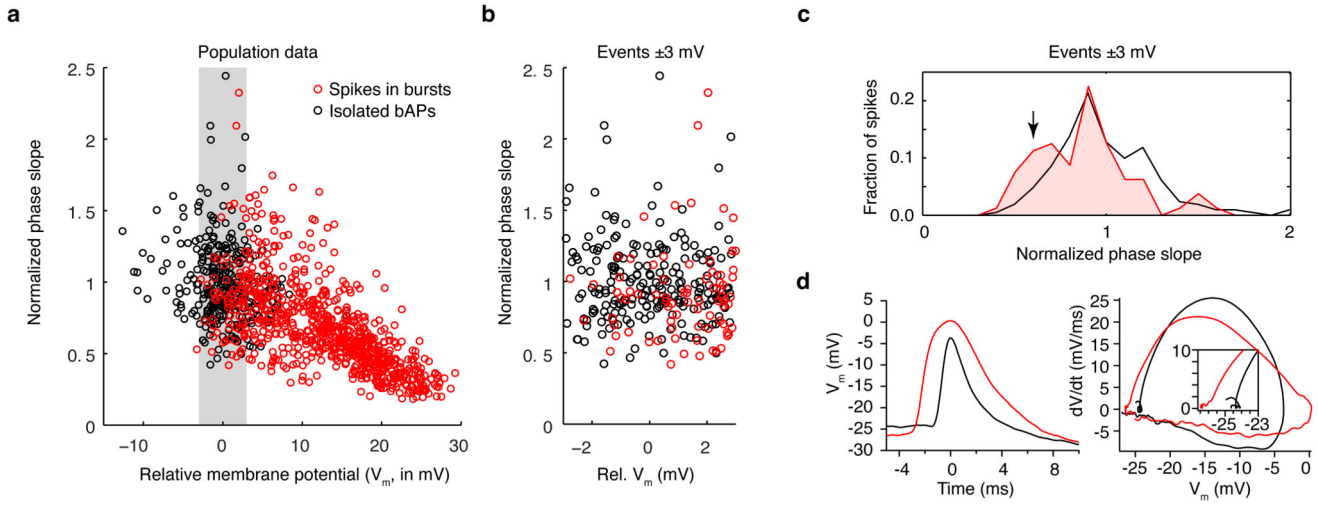

Extended Data Figure 4. The diversity of onset dynamics vs. membrane potential.

a, Spikes (both isolated bAPs, in black, and spikes in dendritic burst events, in red) from each distal dendritic recording were normalized such that isolated bAPs had an mean phase slope of 1. The mean baseline membrane potential (V_m) of isolated bAPs was subtracted from the mean baseline V_m of all spikes. Although many spikes in bursts had depolarized baseline V_ms relative to isolated spikes, there was overlap between the two populations around ± 3 mV. **b**, Expansion of panel a to show spikes at ± 3 mV relative to the mean baseline Vm of isolated bAPs. **c**, Histograms of the two populations reveal a tendency towards lower phase slope values for spikes in bursts ($P = 0.041$; KS test; $n = 211$ bAPs, 80 spikes in bursts). **d**, An example of bAPs and a spike in a burst (both from the same distal dendritic recording) show how although the bAP has a more depolarized baseline V_m, it still

exhibits a steeper phase slope (a kink at the foot of the voltage waveform), indicative of a propagated action potential.

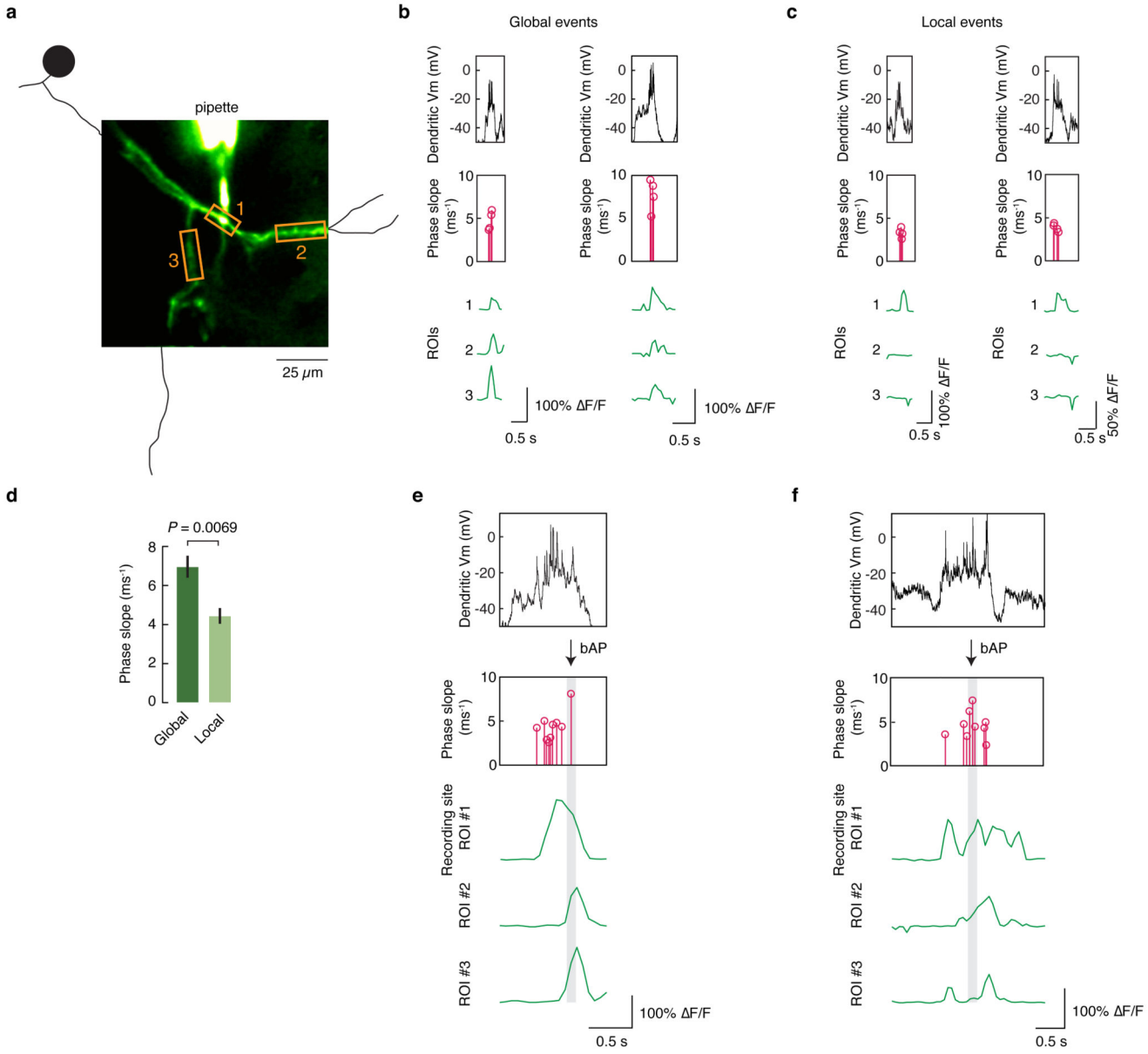

Extended Data Figure 5. Calcium imaging at the site of dendritic recording reveals that global calcium signals are associated with faster onset spikes

a, During dendritic recordings, calcium signals were simultaneously imaged at the site of the recording and nearby dendrites. **b**, In dendritic bursts with global calcium signals that were simultaneously observed at all ROIs, the spikes recorded at the dendrite exhibited steep onsets, indicating that they were likely bAPs. **c**, In local calcium signals that were only observed in the ROI at the site of the recording, the dendritic spikes exhibit slower onsets, indicating that they were likely locally generated. **d**, The maximum phase slope of spikes

Europe PMC Funders Author Manuscripts

occurring during global calcium events was higher than for spikes occurring during local calcium events ($P = 0.0069$, t-test). **e**,**f**, When global calcium signals occurred during ongoing local calcium signals, the initiation was associated with a steep-onset spike.

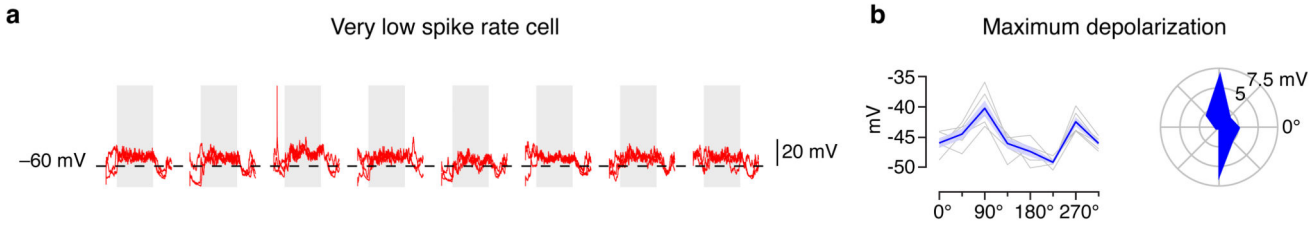

Extended Data Figure 6. Non-firing cells exhibit subthreshold orientation tuning.

a, Raw data for an example cell in which subthreshold orientation tuning is observed although zero spikes were fired during the stimulus presentations. **b**, In this case, the tuning width of the subthreshold membrane potential was quite sharp and confined to two directions.

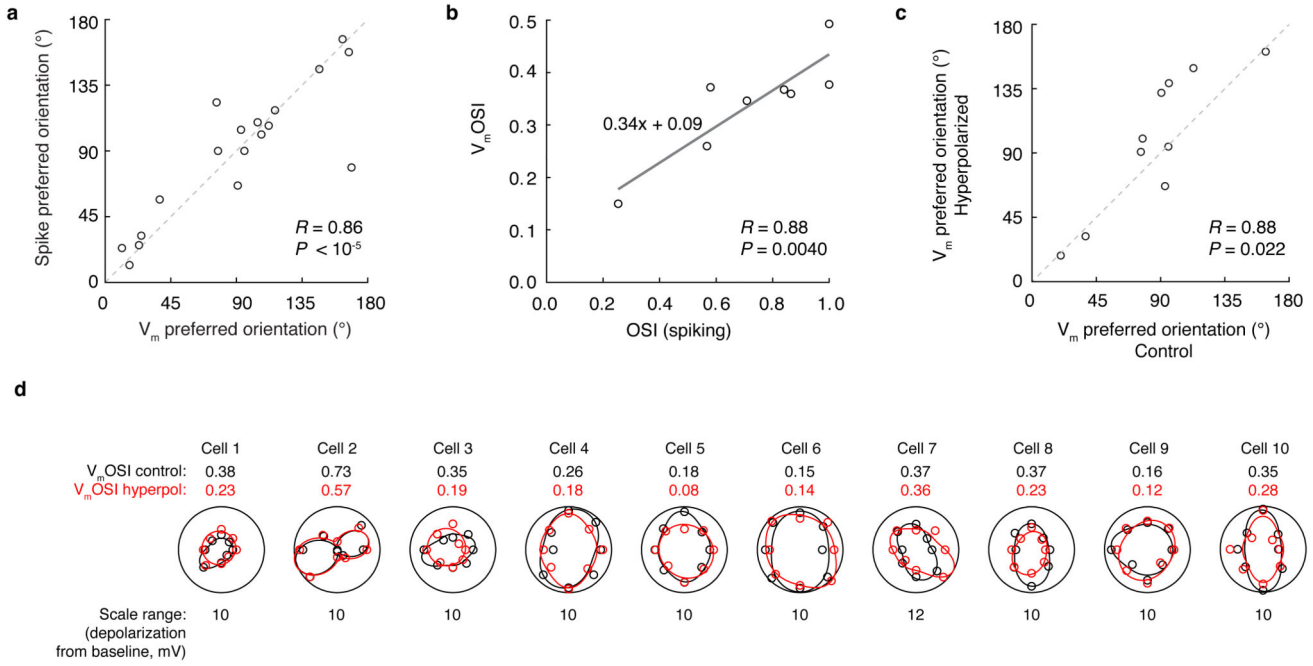

Extended Data Figure 7. Tuning of APs and subthreshold membrane potential.

a, In individual cells, the orientation tuning of spikes and membrane potential were highly correlated, indicating that the tuning of the subthreshold responses was not spurious (mean difference in preferred orientation: 14.8 ± 5.3°). **b**, In individual cells, the orientation selectivity index based on the membrane potential response (V_mOSI) was highly correlated with the conventional spiking-based OSI. **c**, In individual cells, the preferred orientation of the control subthreshold response was correlated with the preferred orientation of the subthreshold response during hyperpolarization. **d**, The black curve is the fitted subthreshold

orientation tuning curve (black circles are raw data points), and the red curve is subthreshold tuning curve during hyperpolarization (red circles are raw data points). The V_mOSI values for control and hyperpolarized conditions are shown next to each plot. The radial axes are linear and start at zero. The maximal radial axis range is shown below each polar plot. The differences in V_mOSI are quantified in Fig. 5g.

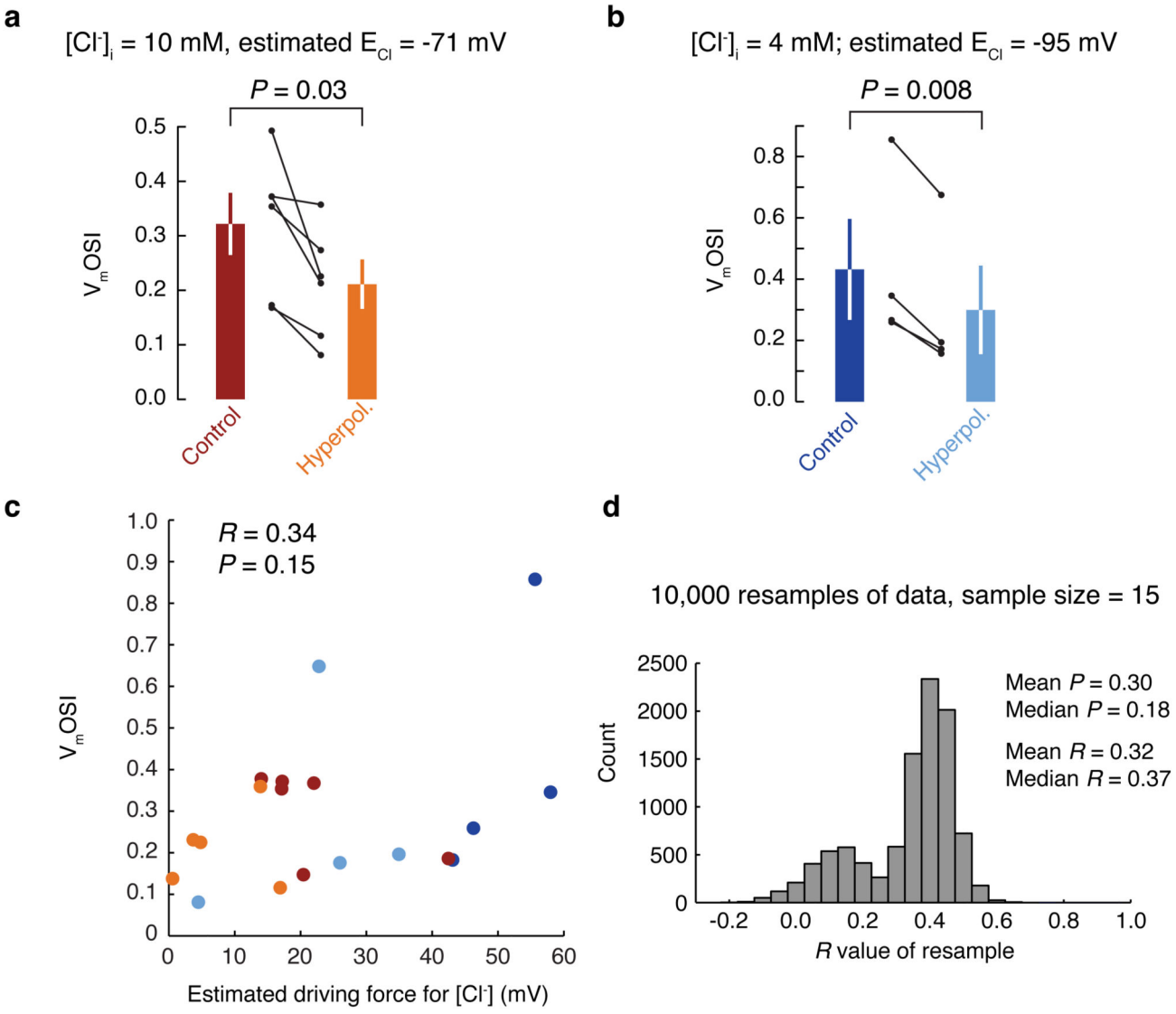

Extended Data Figure 8. Changes in the driving force for chloride do not account for the effects of hyperpolarization on V_mOSI.

a, When the pipette solution contains 10 mM of chloride, the E_{Cl} is estimated to be -71 mV (based on the assumption that natural cerebrospinal fluid contains a similar amount of chloride as the artificial cerebrospinal fluid we use). In this situation, hyperpolarization decreased the orientation selectivity index. **b**, Even with low chloride solution (4 mM; estimated E_{Cl} = -95 mV), the result is the same. **c**, There was not a significant correlation

Europe PMC Funders Author Manuscripts

between the driving force for Cl- and V_mOSI. **d**, Resampling the data (15 of the data points in panel c were selected at random, and the *R* and *P* values for that set of data points were calculated; this process was repeated 10,000 times) confirmed that the result from the correlational analysis in panel c was not biased by a small subset of the data points (the mean *R* and *P* values from the resampling analysis match well with those for the full dataset in panel c).

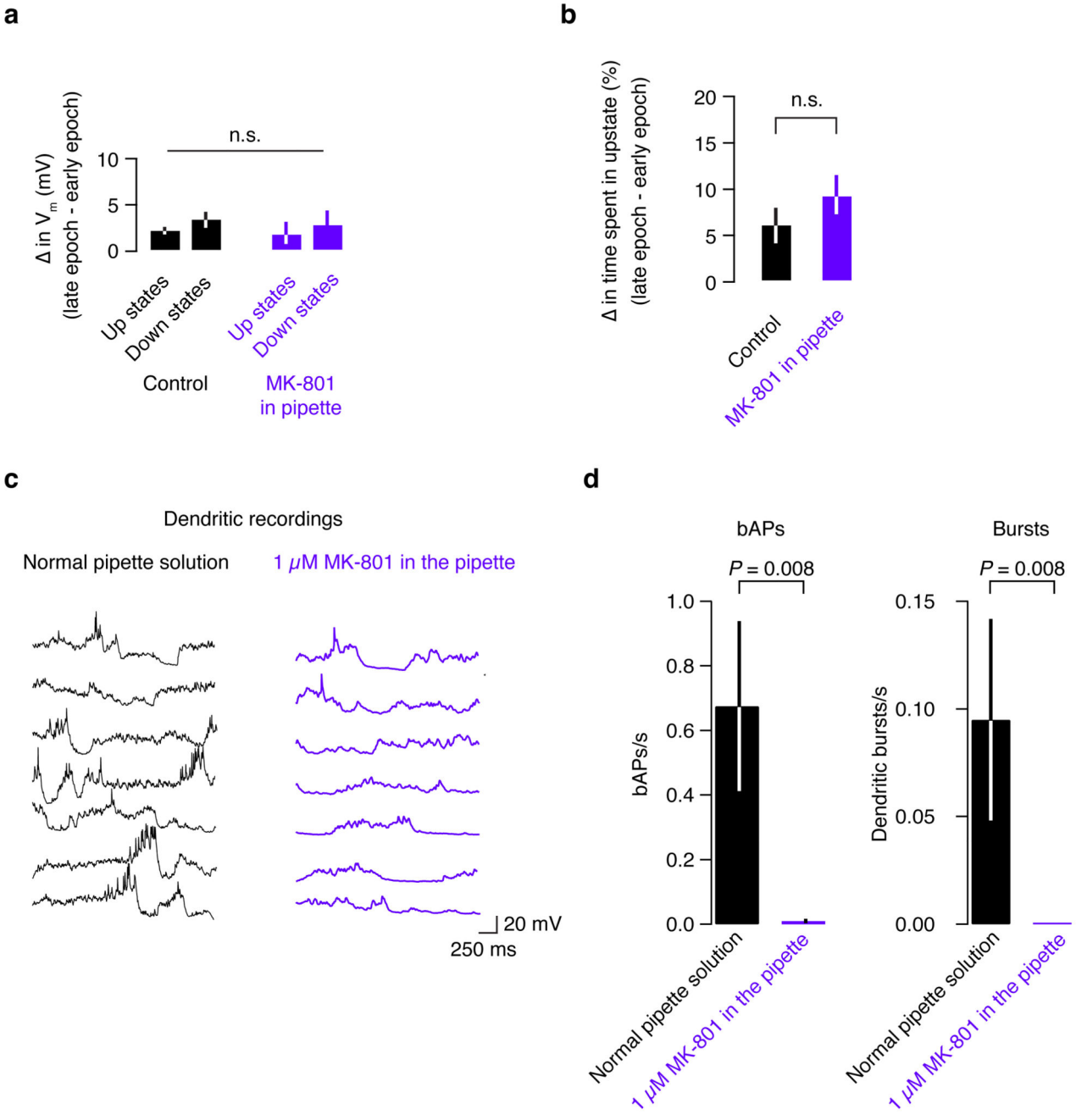

Extended Data Figure 9. The effect of intracellular MK-801 on Up - Down states and dendritic spikes.

Europe PMC Funders Author Manuscripts

a, To determine whether MK-801 that may have leaked out of the pipette during patching affects network circuitry, we examined the dynamics of Up and Down states in our recordings where MK-801 was in the pipette, and control recordings with no MK-801. **b**, Although generally membrane potential drifted up slightly (< 5 mV on average), and time spent in the Up state increased over long recordings (possibly due to the anesthesia wearing off), these trends were identical with or without MK-801 in the patch pipette. **c**, When 1 μM MK-801 was included in the recording pipette, the visually evoked responses contained fewer bAPs and bursts. This trend was clear in a, individual cells, as well as d, across the population. This reduction in spiking confirms that dendritic bursts do not occur when NMDA receptors are blocked. Since the low firing rate in MK-801 recordings prevented a reliable measurement of orientation tuning in the MK-801 dendritic patch recordings, we averaged over all stimulus presentations for both conditions, resulting in a lower average firing rate for bAPs and dendritic bursts.

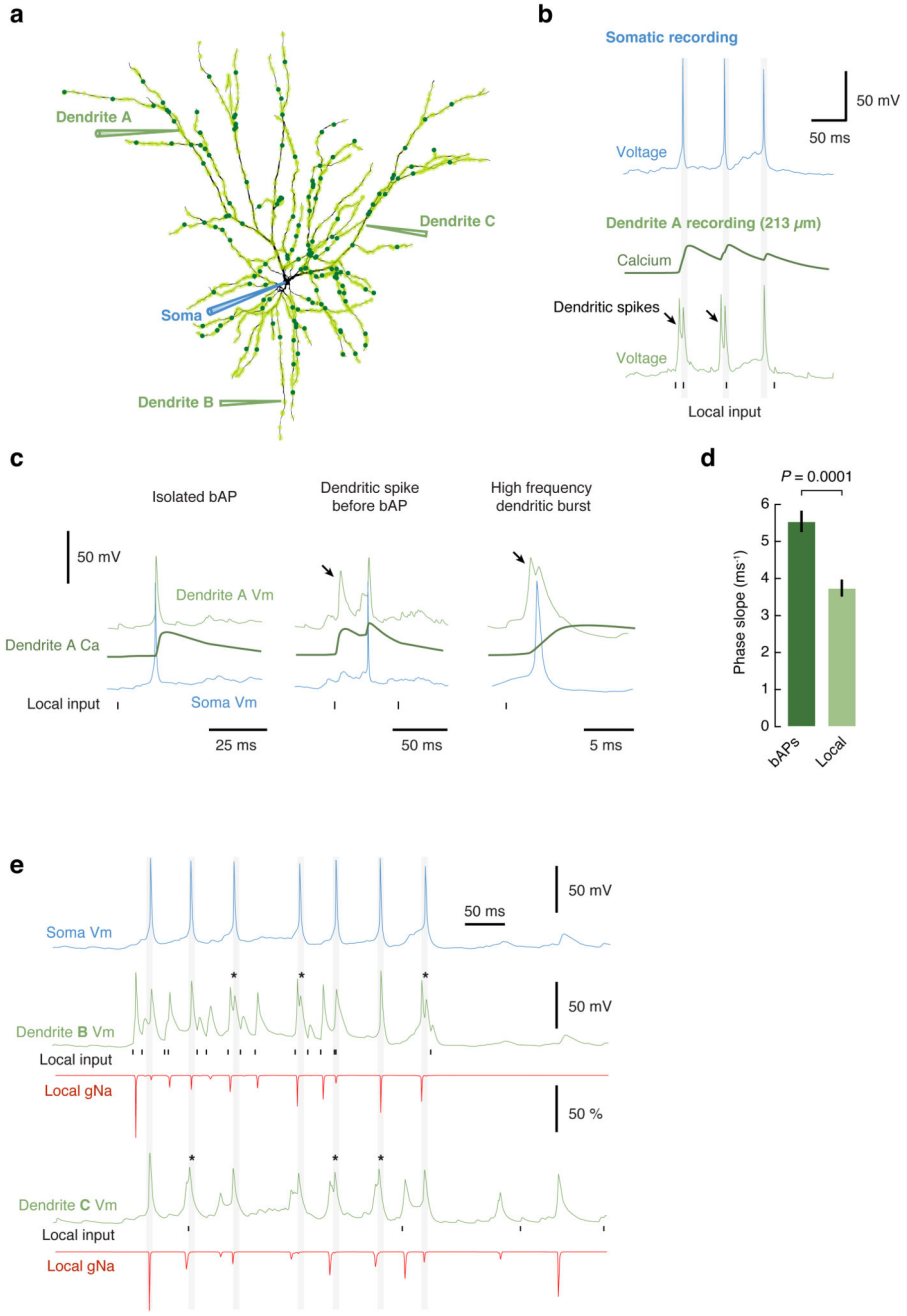

Extended Data Figure 10. Compartmental modeling of dendritic events.

a, A detailed reconstruction of a L2/3 pyramidal cell was used in the simulations. Light green circles over the dendritic tree represent background synapses and dark green are signal synapses (the model had 1100 synapses, not all are illustrated). Voltage was recorded at the soma and at all dendritic branches simultaneously. **b**, Activation of signal synapses at 5 Hz produces high-frequency dendritic bursts, composed of local dendritic spikes and backpropagating action potentials. These bursts were always accompanied by dendritic calcium transients. The timing of activation of excitatory synapses on the recorded dendritic

branch is illustrated. Note how the local EPSPs are clearly smaller than the dendritic spikes. **c**, Examples of specific features consistently observed in the model. Isolated backpropagating action potentials were associated with global calcium transients and had "kinky" onsets. Dendritic spikes often preceded somatic action potentials, had smooth onsets and calcium transients that were localized to the branches where the spikes were recorded, and clearly started before the global transients associated with bAPs. Local dendritic spikes initiated in the dendrite could often be recorded in multiple electrotonically close dendritic branches. Pairs of local spikes and bAPs reached very high frequencies; the example shows a pair at > 400 Hz. When NMDA receptors were removed from the simulations no dendritic spikes were observed and the soma failed to reach threshold for action potential firing. The same occurred when there were no dendritic voltage-activated sodium channels, indicating that the generation of dendritic spikes is required for producing axonal output. **d**, Quantification of spike onset for local dendritic spikes and bAPs in the model reproduced the experimentally observed effect reported in Extended Data Fig. 5d. **e**, Example trial showing the somatic voltage and recordings for two dendrites indicated in panel a. For each dendrite the local voltage, sodium channel conductance (g_{Na}, expressed as a fraction of the maximum conductance) and the timing of activation of excitatory synapses on the recorded dendrite are shown. The g_{Na} traces show that there is significant local sodium channel inactivation after the first spike, and that subsequent spikes are associated with varying degrees of sodium channel conductance. The * symbols show extreme cases when a bAP followed a local dendritic spike at very high frequency and did not recruit any local g_{Na}, therefore indicating that the propagation into the recorded branch was passive.

Supplementary Material

Refer to Web version on PubMed Central for supplementary material.

Acknowledgements

We are grateful to B. Clark, P. Latham, M. London, D. Ringach, A. Roth, C. Schmidt-Hieber and C. Wilms for helpful discussions and for comments on the manuscript. This work was supported by a Long-Term Fellowship and a Career Development Award from the Human Frontier Science Program to S.L.S.; a Helen Lyng White Fellowship to I.T.S.; a Wellcome Trust and Royal Society Fellowship and MRC Programme Leader Track to T.B.; and by grants from the Wellcome Trust, ERC, and Gatsby Charitable Foundation to M.H.

References

1. Johnston D, Narayanan R. Active dendrites: colorful wings of the mysterious butterflies. Trends Neurosci. 2008; 31:309–316. [PubMed: 18471907]
2. London M, Häusser M. Dendritic computation. Annu Rev Neurosci. 2005; 28:503–532. [PubMed: 16033324]
3. Spruston N. Pyramidal neurons: dendritic structure and synaptic integration. Nat Rev Neurosci. 2008; 9:206–221. [PubMed: 18270515]
4. Larkum ME, Zhu JJ, Sakmann B. A new cellular mechanism for coupling inputs arriving at different cortical layers. Nature. 1999; 398:338–341. [PubMed: 10192334]
5. Schiller J, Major G, Koester HJ, Schiller Y. NMDA spikes in basal dendrites of cortical pyramidal neurons. Nature. 2000; 404:285–289. [PubMed: 10749211]
6. Helmchen F, Svoboda K, Denk W, Tank DW. In vivo dendritic calcium dynamics in deep-layer cortical pyramidal neurons. Nat Neurosci. 1999; 2:989–996. [PubMed: 10526338]

7. Llinas R, Nicholson C, Freeman JA, Hillman DE. Dendritic spikes and their inhibition in alligator Purkinje cells. Science. 1968; 160:1132–1135. [PubMed: 5647436]
8. Kamondi A, Acsady L, Buzsaki G. Dendritic spikes are enhanced by cooperative network activity in the intact hippocampus. J Neurosci. 1998; 18:3919–3928. [PubMed: 9570819]
9. Yuste R, Gutnick MJ, Saar D, Delaney KR, Tank DW. Ca2+ accumulations in dendrites of neocortical pyramidal neurons: an apical band and evidence for two functional compartments. Neuron. 1994; 13:23–43. [PubMed: 8043278]
10. Branco T, Clark BA, Häusser M. Dendritic discrimination of temporal input sequences in cortical neurons. Science. 2010; 329:1671–1675. [PubMed: 20705816]
11. Ferster D, Jagadeesh B. EPSP-IPSP interactions in cat visual cortex studied with in vivo whole-cell patch recording. J Neurosci. 1992; 12:1262–1274. [PubMed: 1556595]
12. Volgushev M, Pei X, Vidyasagar TR, Creutzfeldt OD. Postsynaptic potentials in cat visual cortex: dependence on polarization. Neuroreport. 1992; 3:679–682. [PubMed: 1520855]
13. Longordo F, To MS, Ikeda K, Stuart GJ. Sublinear integration underlies binocular processing in primary visual cortex. Nat Neurosci. 2013; 16:714–23. [PubMed: 23644484]
14. Hubel DH, Wiesel TN. Receptive fields of single neurones in the cat's striate cortex. J Physiol. 1959; 148:574–591. [PubMed: 14403679]
15. Larkum ME, Waters J, Sakmann B, Helmchen F. Dendritic spikes in apical dendrites of neocortical layer 2/3 pyramidal neurons. J Neurosci. 2007; 27:8999–9008. [PubMed: 17715337]
16. Waters J, Helmchen F. Background synaptic activity is sparse in neocortex. J Neurosci. 2006; 26:8267–8277. [PubMed: 16899721]
17. Niell CM, Stryker MP. Highly selective receptive fields in mouse visual cortex. J Neurosci. 2008; 28:7520–7536. [PubMed: 18650330]
18. Yu Y, Shu Y, McCormick DA. Cortical action potential backpropagation explains spike threshold variability and rapid-onset kinetics. J Neurosci. 2008; 28:7260–7272. [PubMed: 18632930]
19. Svoboda K, Helmchen F, Denk W, Tank DW. Spread of dendritic excitation in layer 2/3 pyramidal neurons in rat barrel cortex in vivo. Nat Neurosci. 1999; 2:65–73. [PubMed: 10195182]
20. Tan AY, Brown BD, Scholl B, Mohanty D, Priebe NJ. Orientation selectivity of synaptic input to neurons in mouse and cat primary visual cortex. J Neurosci. 2011; 31:12339–12350. [PubMed: 21865476]
21. Jia H, Rochefort NL, Chen X, Konnerth A. Dendritic organization of sensory input to cortical neurons in vivo. Nature. 2010; 464:1307–1312. [PubMed: 20428163]
22. Polsky A, Mel BW, Schiller J. Computational subunits in thin dendrites of pyramidal cells. Nat Neurosci. 2004; 7:621–627. [PubMed: 15156147]
23. Lavzin M, Rapoport S, Polsky A, Garion L, Schiller J. Nonlinear dendritic processing determines angular tuning of barrel cortex neurons in vivo. Nature. 2012; 490:397–401. [PubMed: 22940864]
24. Mel BW. Synaptic integration in an excitable dendritic tree. J Neurophysiol. 1993; 70:1086–1101. [PubMed: 8229160]
25. Smith SL, Häusser M. Parallel processing of visual space by neighboring neurons in mouse visual cortex. Nat Neurosci. 2010; 13:1144–1149. [PubMed: 20711183]
26. Ohiorhenuan IE, et al. Sparse coding and high-order correlations in fine-scale cortical networks. Nature. 2010; 466:617–621. [PubMed: 20601940]
27. London M, Roth A, Beeren L, Häusser M, Latham PE. Sensitivity to perturbations in vivo implies high noise and suggests rate coding in cortex. Nature. 2010; 466:123–127. [PubMed: 20596024]
28. Xu NL, et al. Nonlinear dendritic integration of sensory and motor input during an active sensing task. Nature. 2012; 492:247–251. [PubMed: 23143335]
29. Gentet LJ, et al. Unique functional properties of somatostatin-expressing GABAergic neurons in mouse barrel cortex. Nat Neurosci. 2012; 15:607–612. [PubMed: 22366760]
30. Jiang X, Wang G, Lee AJ, Stornetta RL, Zhu JJ. The organization of two new cortical interneuronal circuits. Nat Neurosci. 2013; 16:210–218. [PubMed: 23313910]
31. Brainard DH. The Psychophysics Toolbox. Spatial Vision. 1997; 10:433–436. [PubMed: 9176952]
32. Pelli DG. The VideoToolbox software for visual psychophysics: transforming numbers into movies. Spatial Vision. 1997; 10:437–442. [PubMed: 9176953]

33. Kitamura K, Judkewitz B, Kano M, Denk W, Häusser M. Targeted patch-clamp recordings and single-cell electroporation of unlabeled neurons in vivo. Nat Methods. 2008; 5:61–67. [PubMed: 18157136]
34. Jahr CE, Stevens CF. Voltage dependence of NMDA-activated macroscopic conductances predicted by single-channel kinetics. J Neurosci. 1990; 10:3178–3182. [PubMed: 1697902]
35. Nevian T, Larkum ME, Polsky A, Schiller J. Properties of basal dendrites of layer 5 pyramidal neurons: a direct patch-clamp recording study. Nat Neurosci. 2007; 10:206–214. [PubMed: 17206140]
36. Spruston N, Jonas P, Sakmann B. Dendritic glutamate receptor channels in rat hippocampal CA3 and CA1 pyramidal neurons. J Physiol. 1995; 482(Pt 2):325–352. [PubMed: 7536248]
37. Pologruto TA, Sabatini BL, Svoboda K. ScanImage: flexible software for operating laser scanning microscopes. Biomed Eng Online. 2003; 2:13. [PubMed: 12801419]
38. Fasano G, Franceschini A. A multidimensional version of the Kolomogorov-Smirnov test. Mon Not R Astr Soc. 1987; 225:155–170.

Europe PMC Funders Author Manuscripts

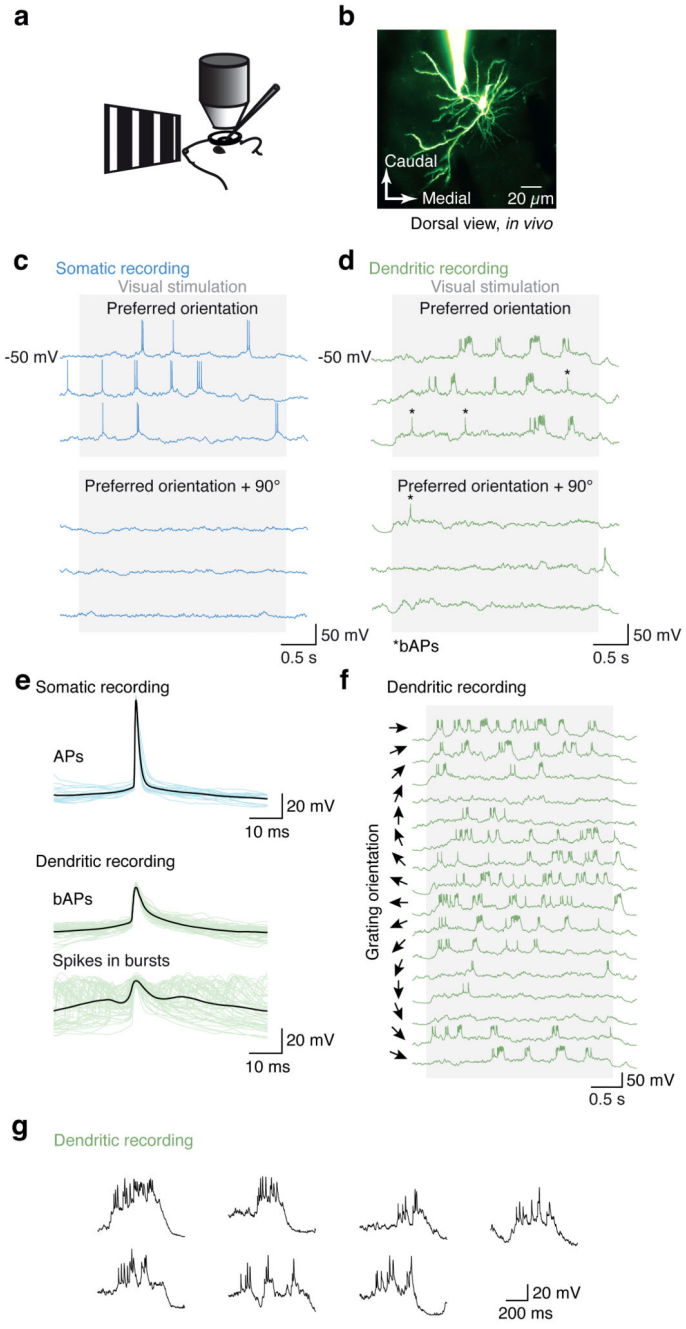

Figure 1. Dendritic patch-clamp recordings from visual cortex pyramidal neurons *in vivo*.

a, Schematic of recording and imaging setup for *in vivo* dendritic patch-clamp recordings under two-photon microscopy. **b**, Two-photon image of a layer 2/3 pyramidal neuron in mouse visual cortex *in vivo* filled with Alexa 594 via a dendritic patch-clamp recording 100 μm from the soma (maximum intensity projection). **c**, Somatic spiking and dendritic activity (**d**) evoked by presenting square wave grating visual stimuli both exhibited reliable, orientation-tuned burst spiking events. The asterisks mark bAPs. **e**, Spikes within dendritic burst events were highly variable compared to the more stereotyped bAPs and somatically

recorded APs. **f**, Dendritic burst event frequency varied with orientation. **g**, individual burst events were highly variable in amplitude and kinetics (dendritic recording 150 μm from the soma).

Europe PMC Funders Author Manuscripts

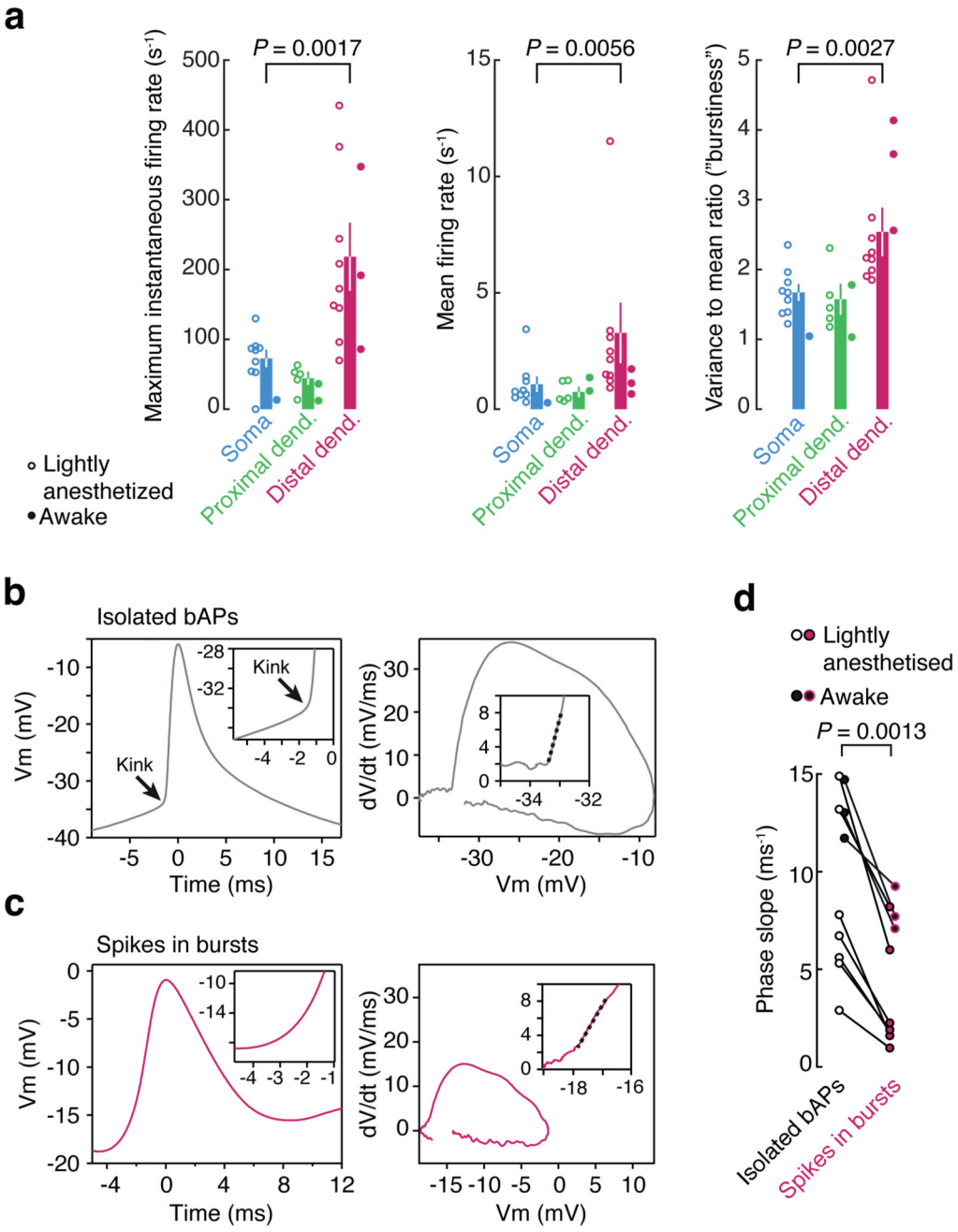

Figure 2. Visually evoked dendritic burst events are local.

a, Whole cell patch clamp recordings were performed at the soma ($n = 9$), proximal dendritic locations (< 50 μm from soma; $n = 5$), or distal dendritic locations (> 75 μm from soma; $n = 9$). Stimulus-evoked event frequency at the soma and proximal dendritic locations were similar. However, event frequency and burstiness (variance-to-mean ratio, or Fano factor) was significantly higher at distal dendritic locations. (*P*-values from the Wilcoxon rank sum test). Data from awake recordings (filled circles, $n = 6$ total) exhibit the same trends. **b**, The inflection in membrane potential for backpropagated spikes recorded at distal

dendritic locations (> 100 μm from the soma) exhibited a sharp kink, consistent with propagated spikes, as visible both in voltage vs. time plots (left), and dV/dt vs. voltage phase plots (right). **c**, By contrast, spikes in bursts exhibited a slower onset, consistent with local generation. **d**, Across the population of dendritic recordings, isolated spikes consistently exhibited sharper inflections at onset (measured as the initial slope in the dV/dt vs. voltage phase plots; dashed lines in b and c) than spikes in bursts. Distal dendritic recordings from awake mice (black-filled symbols) exhibited the same trend.

Europe PMC Funders Author Manuscripts

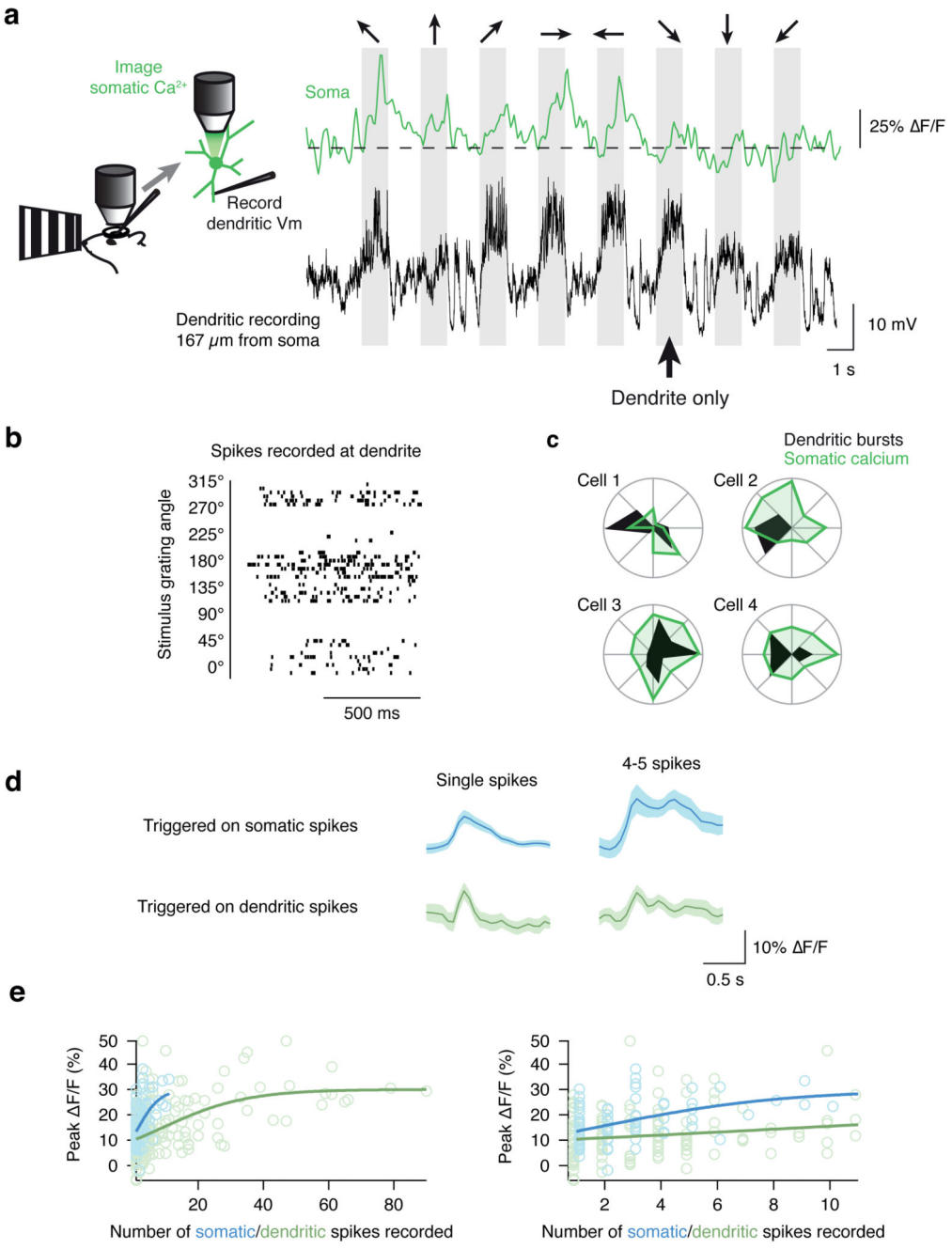

Figure 3. Simultaneous dendritic recording and calcium imaging at the soma shows that dendritic bursts are local.

a, To infer spiking activity at the soma during dendritic patch recordings, neurons were filled with a calcium indicator and somatic calcium signals were imaged. During simultaneous dendritic voltage recordings and somatic calcium imaging, dendritic bursts were sometimes not accompanied by robust somatic calcium signals (marked with an arrow). **b**, Dendritic bursting was well tuned, and (**c**) overlapped with the orientation tuning at the soma (data from Cell 1 is shown in panels a and b). **d**, To calibrate the calcium signals seen at the soma,

we generated spike-triggered averages of the somatic calcium signal for well-isolated single spikes, and bouts of 4-5 spikes (within 640 ms). The somatic calcium signal amplitude was similar for single spikes whether the spikes were recorded at the soma or the dendrite. For bouts of 4-5 spikes recorded at the dendrite, no difference was found compared to single spikes recorded at the soma, suggesting that some dendritic spikes were local. **e**, Across the population of events, even though the calcium signals saturated around the same magnitude (~ 0.3 ΔF/F, not different between the two configurations, $P = 0.99$), the somatic calcium signal as a function of number of dendritic spikes rose much more slowly than that for somatically-recorded spikes. The right-hand plot shows an expansion of the x-axis to highlight the data from responses with < 10 spikes.

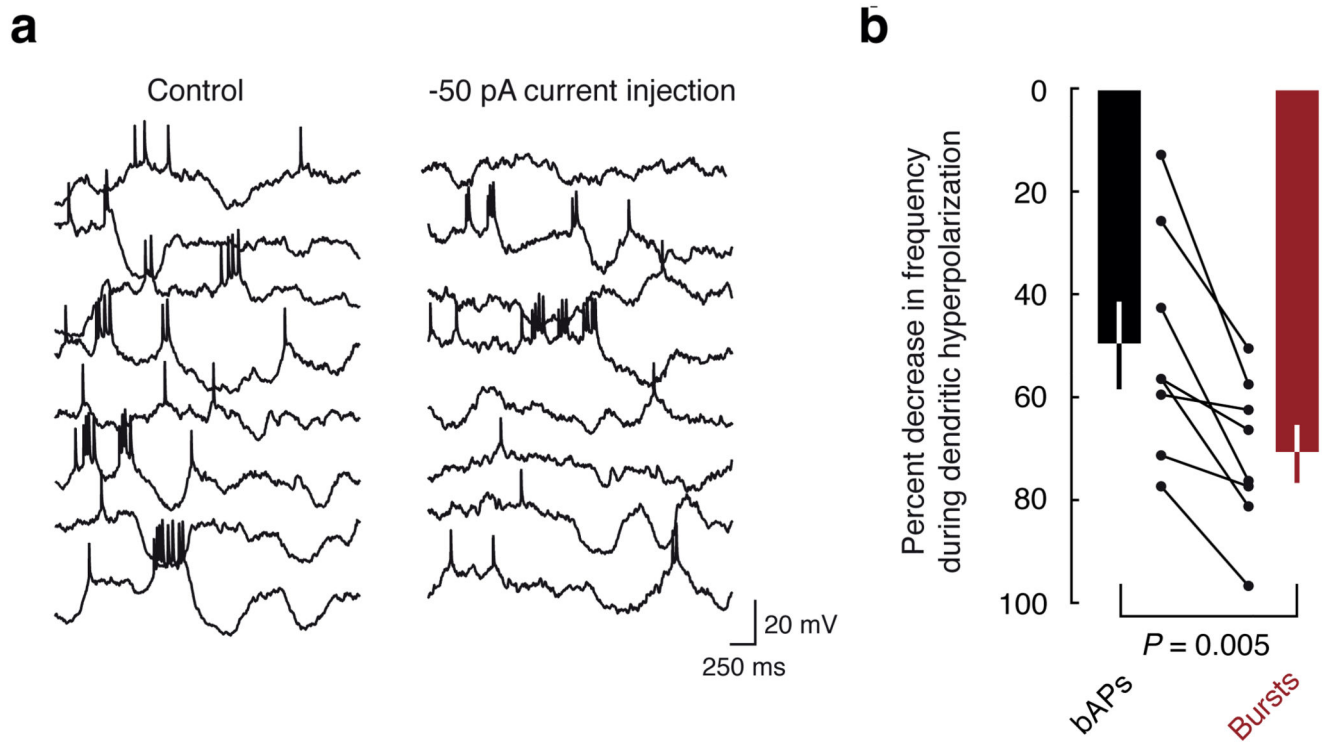

Figure 4. Hyperpolarization decreases the frequency of dendritic bursts.

a, An example dendritic recording shows that hyperpolarization decreased the frequency of bursts (from 0.32 Hz to 0.14 Hz; -68%) more than the frequency of bAPs (0.51 Hz to 0.36 Hz: -30%). **b**, Population data showing that bursts and bAPs are both suppressed ($P = 3.0 \times 10^{-6}$, and $P = 0.0004$, respectively, t-test), and bursts are suppressed to a greater degree than bAPs by hyperpolarization ($P = 0.005$, paired t-test).

Europe PMC Funders Author Manuscripts

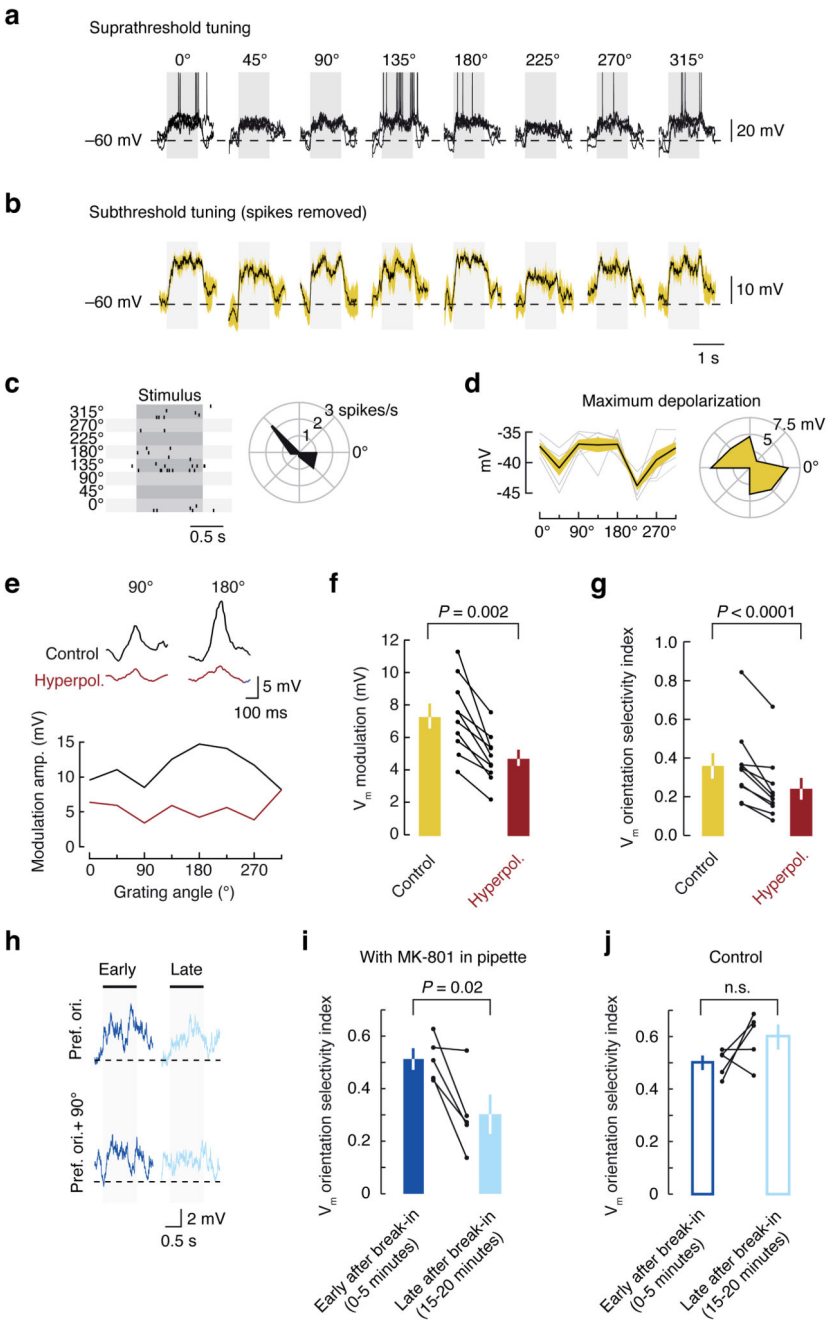

Figure 5. Dendritic mechanisms contribute to the selectivity of subthreshold orientation tuning.

a, Somatic whole cell recording from a layer 2/3 pyramidal neuron, exhibiting robust visually-evoked spiking (3 sweeps overlaid; stimulus duration indicated by grey bar) and **b**, subthreshold responses (50 ms windows around spikes were blanked, and the same results were obtained when blanking window was decreased to 20 ms) which were orientation tuned as evidenced by **c**, spikes rasters, and **d**, polar plots of maximal depolarization. **e,** Hyperpolarization decreased the amplitude of the stimulus-evoked membrane potential modulation, and decreased its tuning selectivity. Hyperpolarization decreased **f,** V_m

modulation amplitude and **g**, orientation selectivity index across the population. To investigate the mechanisms involved in the dendritic spike contributing to orientation tuning, whole cell somatic patch clamp recordings were performed with 1 μM MK-801 in the pipette solution. **h**, Orientation tuning selectivity progressively decreased during the recording as MK-801 diffused into the cell and blocked NMDA channels. In these example traces, the response to the preferred orientation decreased from early in the recording to late in the recording. **i**, Across the population, subthreshold orientation tuning was strongly inhibited at late time points in the recording, compared to early time points. **j**, In control recordings, with no blockers in the pipette solution, orientation tuning selectivity was not significantly different ($P > 0.05$, two sample t-test) from the early period of MK 801 recordings. Furthermore, tuning did not significantly change during long recordings.